ACS APPLIED MATERIALS & INTERFACES

Letter

www.acsami.org

Direct Immersion Annealing of Thin Block Copolymer Films

Arvind Modi,[†] Sarang M. Bhaway,[†] Bryan D. Vogt,[†] Jack F. Douglas,[‡] Abdullah Al-Enizi,[§] Ahmed Elzatahry,[∥] Ashutosh Sharma,[⊥] and Alamgir Karim*[,†]

[†]Department of Polymer Engineering, University of Akron, Akron, Ohio 44325, United States

[⊥]Department of Chemical Engineering, Indian Institute of Technology Kanpur, Kanpur, Uttar Pradesh 208016, India

[‡]Materials Science and Engineering Division, National Institute of Standards and Technology, Gaithersburg, Maryland 20899, United States

[§]Chemistry Department, Faculty of Science, King Saud University, Riyadh 11451, Saudi Arabia

[∥]Materials Science and Technology Program, College of Arts and Sciences, Qatar University, PO Box 2713, Doha, Qatar

Supporting Information

ABSTRACT: We demonstrate ordering of thin block copolymer (BCP) films via direct immersion annealing (DIA) at enhanced rate leading to stable morphologies. The BCP films are immersed in carefully selected mixtures of good and marginal solvents that can impart enhanced polymer mobility, while inhibiting film dissolution. DIA is compatible with roll-to-roll assembly manufacturing and has distinct advantages over conventional thermal annealing and batch processing solvent-vapor annealing methods. We identify three solvent composition-dependent BCP film ordering regimes in DIA for the weakly interacting polystyrene–poly(methyl methacrylate) (PS–PMMA) system: rapid short-range order, optimal long-range order, and a film instability regime. Kinetic studies in the "optimal long-range order" processing regime as a function of temperature indicate a significant reduction of activation energy for BCP grain growth compared to oven annealing at conventional temperatures. An attractive feature of DIA is its robustness to ordering other BCP (e.g. PS-P2VP) and PS-PMMA systems exhibiting spherical, lamellar and cylindrical ordering.

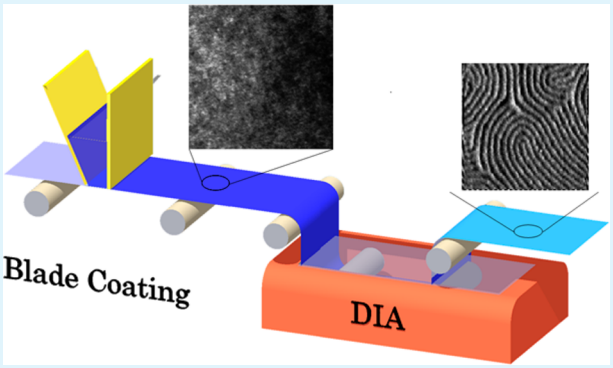

KEYWORDS: *mixed solvents, direct immersion annealing, block copolymer ordering, kinetics*

Self-assembled block copolymer (BCP) templates are promising candidates for nanofabrication, but their rapid and inexpensive scale-up is challenging in comparison to conventional top-down methods, e.g., photolithography.[1] BCP thin films can enable potential applications by enabling platforms such as substrate supported nanodots[2−6] for nano-optics, nanowires[4,7,8] for electronic devices, nanoporous membranes[9,10] for water–oil separation, and energy harvesting plasmonic devices.[11−14] Most applications require a tight control over grain and microdomain size and orientation of self-assembled blocks relative to the substrate, which may be aided by external fields such as shear,[15−18] chemical[19] and physical[20,21] patterning, and other techniques.[22]

BCP films cast from fast evaporating solvents at room temperature typically results in films trapped in a quenched nonequilibrium morphology lacking long-range order[23] due to film vitrification. Control of the subsequent annealing conditions to obtain the desired ordered BCP morphology is key to achieving a target degree of ordering. Thermal annealing involves simply heating the BCP films above the glass transition temperature (T_g) of both blocks to provide sufficient mobility to allow BCP ordering on a reasonable time scale. Thermal annealing can be problematic if one or more blocks can crystallize or if the blocks chemically degrade at the elevated annealing temperatures.[24] The slow diffusion of high molecular mass polymers also greatly increases the BCP film processing time.[26] Solvent vapor annealing (SVA)[23] of BCP films overcomes some of the drawbacks of thermal annealing, but can introduce new challenges. The thin films swell when exposed to vapor where the extent of swelling depends on the nature and amount of solvent adsorbed. Unfortunately, film swelling can lead to a number of undesirable effects that are difficult to control. The extent of film swelling resulting from these processing conditions can affect morphology, domain size, and the orientation of BCP morphology with respect to substrate.[23] Other effects can include dewetting, differential block swelling, and shifts of order–disorder or order–order transitions that depend sensitively upon the solvent and processing conditions.[23] Well-ordered BCP films are often

Received: July 14, 2015
Accepted: September 9, 2015
Published: September 9, 2015

DOI: 10.1021/acsami.5b06259
ACS Appl. Mater. Interfaces 2015, 7, 21639−21645

obtained by quenching SVA ordered and swollen films, but the time scales required to achieve this ordering vary significantly, ranging on the order of few minutes to several days. These complications in thermal melt annealing and SVA processing leads us to consider other more effective strategies for enhancing the ordering of glassy BCP films on time scales and methods appropriate for commercial processing applications.

Kim et al.[26] showed that SVA, followed by thermal annealing, allowed for greatly enhanced ordering in high-molecular-mass BCPs in comparison to the individual methods. However, most SVA setups require a robust control over the solvent vapor environment, since the swollen film thickness is highly sensitive to the solvent vapor pressure and the temperature of substrate and surrounding environment.[27] Moreover, there is a "dead" processing time during which the vapor phase equilibrates within the polymer film in the processing chamber that often leads to long processing times. Although this synergistic use of solvent annealing and thermal annealing seems to be a step in the right direction, the processing method still has the inherent processing difficulties of SVA.

Sharma et. al[28−31] have recently demonstrated that direct immersion of thin homopolymer films in solvent mixtures allows for a fine control of the scale of the resulting dewetting patterns. In this thin film processing method, the solvent mixture provides both an enhanced mobility, required for enhancing the film dewetting kinetics,[28−32] and serves to reduce the film interfacial tension, a thermodynamic factor relating to the pattern formation. An extension of this approach to PS−PDMS block copolymers, a BCP having a high block−block interaction parameter in the bulk ($\chi \approx 0.2$), was investigated by Jung et al.,[33] who found that the use of mixed solvents could lead to enhanced BCP ordering. However, Jung et al.[33] also reported that this processing method is not without its complications; BCP films in their study were found to be generally unstable after immersion and underwent a complex morphological evolution depending on immersion time, temperature and solvent composition. In this method of processing, the complications of film swelling are exchanged for those associated with film dissolution. Nonetheless, direct immersion annealing with mixed solvents seems to be very promising method, prompting the present work exploring whether a more judicious choice of solvent mixture might allow for better control of the polymer ordering and prevention of the dissolution process.

Here we show that direct immersion annealing (DIA) of BCP films can be effectively controlled to rapidly achieve well-ordered thermodynamically stable bulk morphology having long-term stability if the solvent mixture is chosen appropriately. In particular, a poor solvent is chosen as one of the solvents to regulate the rate of polymer film dissolution, along with a good solvent that imparts high degree of mobility within the film. The overall mixture then maintains a finite interaction parameter for microphase separation of the BCP, even for a weakly segregated BCP system such as polystyrene-*b*-poly(methyl methacrylate) (PS−PMMA) ($\chi \approx 0.037$). Such BCP systems are more difficult to control than more strongly segregated ($\chi > 0.1$) systems by DIA. Furthermore, an important aspect of this new form of DIA, is that the ordered morphologies are rapidly obtained, yet they are stable after extended immersion times in our solvent mixtures. Finally, we find the morphologies developed under DIA closely accord with predicted equilibrium BCP morphologies and demonstrate it to be broadly applicable to a range of PS−PMMA morphologies, and a strongly segregated polystyrene-*b*-poly(2-vinylpyridine) (PS-P2VP) BCP system as well. In particular, we apply DIA to a variety of PS−PMMA BCP morphologies by varying block compositions to yield spherical, cylindrical, and lamellar morphologies. Thus, DIA with carefully selected solvent mixtures appears to be broadly applicable to controlling ordering of BCP systems under reasonable processing conditions.

For measurements on the kinetics of BCP ordering using DIA, we prepared films of the well-known weakly segregated BCP system, PS−PMMA (47.5 kg/mol, $f_{PS} = 0.74$, referred as *Cyl47*) with thickness ($h \approx 44$ nm; $1.63L_0$, $L_0 \approx 27$ nm) exhibiting a cylindrical morphology on Si substrate wafers with the native SiO_2 layer exposed to 2*h* UVO for cleaning purposes. PS−PMMA films were initially flow coated on the wafers from 2 to 3 mass % toluene solutions, to fabricate as-cast films that are in a quenched-disordered state. For the DIA processing, we utilized freshly prepared mixtures of *n*-heptane (hereafter heptane) and acetone at various mole fractions over a broad range of composition. All solvent mixtures (SM) correspond to mixtures of heptane and acetone and their molar composition is indicated as acetone mole fraction, referred to as x_{ace}, unless otherwise specified. The solvent mixture choice is based on solubility parameters of the solvents, considering the dispersion (δ_d), hydrogen-bonding (δ_h), and polar (δ_p) components of the Hansen solubility parameter of n-heptane and acetone to be (15.3, 0.0), (0.0,15.5), and (10.4, 7.0) ($MPa^{0.5}$), respectively.[34] While heptane is a nonsolvent for both PS and PMMA, acetone is a good solvent for PMMA and a marginal solvent for PS. Hence, acetone only plasticizes the PS block to a limited extent, but sufficiently for enhancing overall BCP mobility. Further, heptane and acetone are completely miscible in the measured temperature range as we vary the solvent mixture composition, so that the solvent mixture is homogeneous. Solubility parameters are useful in determining the choice of solvent for low χ systems because nearly equally good solvent for both blocks can significantly reduce χ between the blocks adversely affecting the BCP ordering driving force. Although this may seem like an unfavorable situation, lowering the χ to weak segregation regime can accelerate the kinetics of defect removal for long-range order, a concept of much interest for BCP systems recently.[35] The choice of nonsolvent is to primarily prevent detachment or complete dissolution of films from the substrate. However, the nonsolvent should be such that it should not drastically lower the solvent quality needed for the swelling induced mobility for ordering of the BCP. It has been observed that small molecule alcohols, e.g., methanol or ethanol, in spite of being nonsolvents for the BCP system, are not suitable because of their high mobility and substrate wetting induced film delamination.[36] To explore the solvent quality effect, we considered a wide range of solvent mixture compositions in our analysis below.

Prior to DIA, the as-cast dry state films were independently brought to the desired solvent mixture (SM) immersion temperatures (22 °C (295 K), 35 °C (308 K), 45 °C (318 K), and 56 °C (329 K)), that are well below the BCP T_g. (AFM height sensor image of typical as-cast dry state film showing uniform surface with Rms roughness <1 nm cast from toluene solution at room temperature is shown in Figure S7.) Immersed films were removed from the temperature controlled SM after an "annealing time" and any potential residual solvent was subsequently removed using a hot-plate kept at 60 °C, well

DOI: 10.1021/acsami.5b06259
ACS Appl. Mater. Interfaces 2015, 7, 21639−21645

below the T_g of both blocks to vitrify the BCP morphology. To verify that the residual solvent evaporation process had negligible effect on the morphology of the thin films, we rinsed some SM immersed films with a nonsolvent, pure heptane to remove excess acetone from the DIA films, and then dried on a hot-plate at 60 °C. No difference was observed in the morphology of these thin films as compared to direct hot-plate dried films.

Figure 1 shows AFM images of *Cyl47* BCP films annealed in a *SM* (x_{ace} = 0.33) for different durations of time, from 12 s to

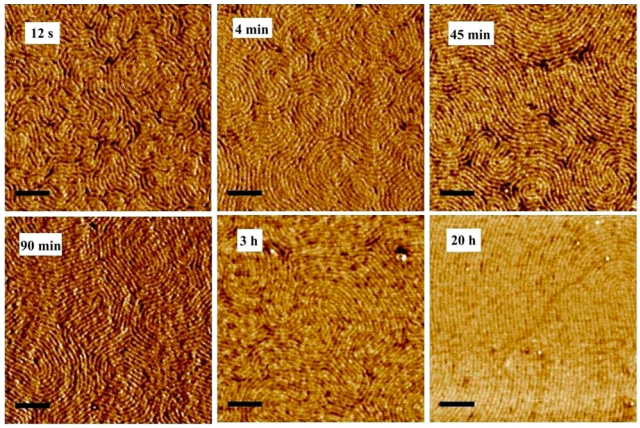

Figure 1. AFM Phase images of *Cyl47* films (≈ 44 nm) annealed in SM (x_{ace} = 0.33) for different duration of time (mentioned in inset) at room temperature (295 K) (scale bar: 250 nm).

20 h, at T = 295 K (22 °C). The BCP grain size increases while the defect density decreases with increase in immersion time in the solvent mixture. We note that even at a short annealing time of 12 s, the BCP cylinder structure is well developed. Comparatively, it would take several hours oven annealing at modest elevated temperatures above T_g (≈100 °C) to obtain an equivalent grain size. Undoubtedly, increasing the annealing time in SM increases the grain size and correlation length of the BCP cylinders, and we next quantify this effect.

Figure 2A shows that the PMMA cylinder orientation correlation function (ξ) (calculated from method discussed in ref 37) is related to immersion time[37] t as $\xi(t) = \xi_0(T,n)t^n$, where ξ is the orientation correlation function, T is the absolute temperature, and n is the power law exponent.[25] Orientation correlation length (ξ) for a sample (ordered block copolymer thin film in our case) is the characteristic length scale (domain spacing for the cylinder forming block copolymer) over which correlation orientational order parameter ($\psi(\mathbf{r}) = e^{i2\theta(r)}$) decays. It is obtained by fitting orientational correlation function ($g(\mathbf{r}) = \langle \psi(0)\psi(\mathbf{r}) \rangle$) to a radially decaying exponential function ($e^{-r/\xi}$).[37] We clarify that the $\xi_0(T,n)$ prefactor is a direct measure of how fast the early stage morphology evolution is. Previous[37] studies of PS−PMMA, *Cyl47*, h ≈ 170 nm thick film annealed under uniform oven annealing at 180 °C suggested $\xi(t) \approx 15.48t^{0.25}$ (nm). By comparison, ξ_0 is much higher in DIA, $\xi(t) \approx (122 \pm 23)t^{0.14\pm0.03}$ (nm) for T = 329 K (56 °C), and the average domain growth exponent over all temperatures is larger, $< n > \approx 0.17$. DIA thus leads to a 3 to 8 fold increase in the early stage ξ_0 (Figure 2B) *development* compared to uniform oven annealing,[37] depending on the *SM* temperature. It is interesting to observe close similarity of ξ_0 and $\langle n \rangle$ of DIA with recent work by Yager et al.,[38] $\xi(t) \approx (116 \pm 10)t^{0.14\pm0.01}$ in 170 nm thick PS−PMMA (31.6−17.5) kg/mol films, oven

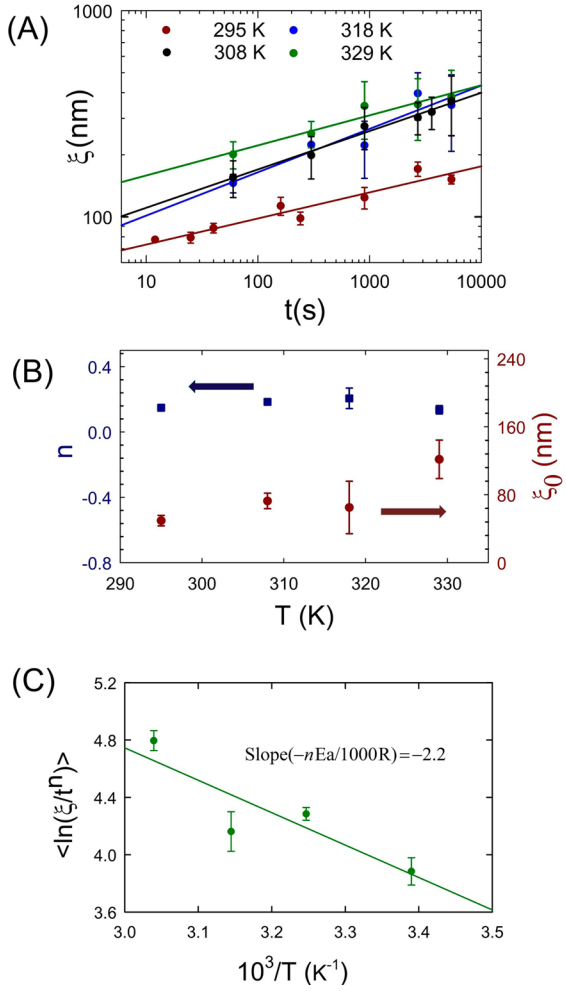

Figure 2. (A) Correlation length (ξ) as a function of time (t) at 295, 308, 318, and 329 K. (B) Exponent (n) and prefactor (ξ_0) as a function of temperature. (C) Time-averaged normalized correlation length as a function of temperature for ∼44 nm thick film of *Cyl47* on Si substrate annealed in SM (x_{ace} = 0.33) where $E_a \approx 111 \pm 63$ kJ/mol. For all figures, uncertainty corresponds to one standard deviation.

annealed at a fairly high temperature of 240 °C. As in DIA, there is a significant increase in the prefactor of the grain growth scaling relation $\xi(t)$, but this process lowers growth exponent (i.e., $n = 0.14 \pm 0.01$ at 240 °C), presumably because of the reduction of the χ parameter at the elevated temperature. At lower temperature of 200 °C, we note that growth exponent is higher, i.e., $n = 0.27 \pm 0.04$ as also observed by Yager et al.[38] Thus, our DIA conditions appear to be equivalent to high-temperature melt annealing BCP conditions by analogy.

Figure 2C shows the activation energy (E_a) for grain growth in DIA, calculated by fitting $\xi_0(T)$ to an Arrhenius equation

$$< \frac{\xi(T)}{t^n} > = Ae^{-nE_a/RT}$$

where the activation energy is estimated to equal 111 ± 63 kJ/mol. Notably, the determined activation energy is lower than defect diffusion activation energy of 270 kJ/mol reported by Ruiz et al.[25] for cylinder forming PS−PMMA in thin films melts. However, it coincidentally accords well with a lower value of 122 kJ/mol for thermally annealed PS−PMMA (91 kg/mol, f_{PS} = 0.75)[39] in the bulk state.

DOI: 10.1021/acsami.5b06259
ACS Appl. Mater. Interfaces 2015, 7, 21639−21645

For an "optimal' choice of SM, in situ swelling measurements were performed using an ellipsometric liquid cell attachment that allowed for data collection at a fixed angle (75° relative to the normal from the film surface), whereas the films were immersed in the SM at room temperature. The swollen film thickness was determined using the Cauchy model for optical properties of BCP films, while accounting for changes in ambient refractive index upon immersion of the film in the SM. From ellipsometric measurements, a film swelling ratio, SR (= h/h_o) was determined, where h and h_o are film thickness in swollen and dry state, respectively.

We observe that the films swell immediately (<3 s) upon immersion in the solvent mixture irrespective of solvent mixture composition. The films attain an equilibrium swollen thickness (h) within 1 min of injection of solvent into liquid cell, whose value primarily depends on the solvent mixture composition (Figure 3). Even pure heptane [SM (x_{ace} = 0)],

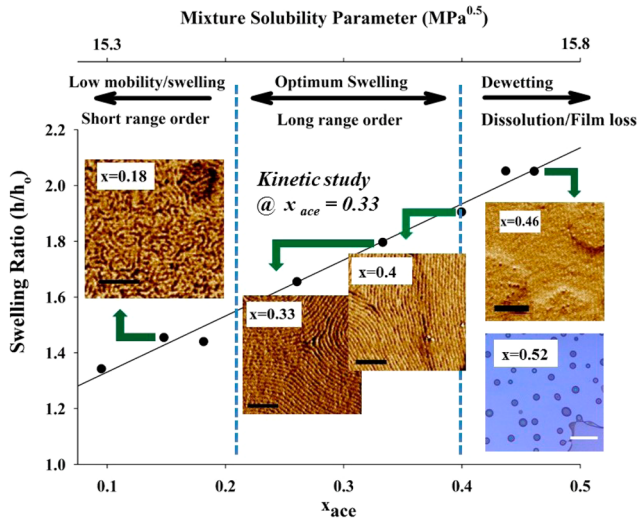

Figure 3. Graph showing a linear relation between swelling ratio (SR) vs acetone mole fraction (x_{ace}) for a DIA immersion time of 3 min. Fitted equation: SR = h/h_0 = 2.01x_{ace} ± 1.13. Illustrative long-time AFM phase images in the graph show *Cyl47* direct immersion annealed in different solvent mixtures (scale bar: 250 nm). Optical microscope image (scale bar: 20 μm) in dissolution/dewetting regimes is shown.

despite being a nonsolvent, swells the films by a nominal amount (≈ 4 nm) due to "weak plasticization" of the top layer by heptane[40,41] attributed to entropic effects. We expect that acetone (which has higher affinity for both PMMA and PS than heptane) competitively segregates at the polymer−liquid interface, so that the swelling is primarily due to acetone in mixed solvent cases.

Expectedly, the overall Hansen solubility parameter (HSP) of the solvent mixture varies with different heptane/acetone composition ranging between 15.3 $MPa^{0.5}$ < δ_{total} < 19.9 $MPa^{0.5}$ for 0 < x_{ace} < 1. In this range of solvent mixtures for the given PS−PMMA *Cyl47* system, we observe three regimes of swelling behavior: (a) Low mobility/short-range ordering regime characterized by 1 ≤ SR ≤ 1.5 for 0 ≤ x_{ace} ≤ 0.2. Here, representative AFM phase image (Figure 3), for x_{ace} = 0.18, shows poorly correlated structures, and high defect density due to limited swelling (low solvent uptake) and hence, low mobility. (b) Optimum swelling regime with 1.5 < SR < 1.9 for 0.2 ≤ x_{ace} ≤ 0.4, indicative of higher acetone uptake. Here, representative AFM phase image as shown in Figure 3, for x_{ace} = 0.33 exhibit much larger correlation length scales and significantly reduced defect counts per unit area. Our kinetic study is performed in a regime in which the BCP morphologies are stable. (c) Dewetting/dissolution regime characterized by BCP film dewetting or dissolution with time. A transition from long-range ordering to dewetting/dissolution regimes occurs approximately under the following condition

$$\sqrt{\delta_{h,mixture}^2 + \delta_{p,mixture}^2} \approx \sqrt{\delta_{h,PS}^2 + \delta_{p,PS}^2}$$

when SR > 1.9 for x_{ace} > 0.4. As the acetone concentration increases, the polar and hydrogen bonding components of HSP increases (Figure S1). This correlation of HSP with acetone content indicates that dewetting/dissolution transition is observed above the solubility limit where the hydrogen bonding and polar component of solubility parameter nearly approach respective solubility parameters of the majority block, PS in this case. This upper limit of solvent mixture quality variation allows for extension (initial solvent mixture and composition selection) of direct immersion annealing to other BCP or polymeric systems. The upper limit for SM quality for DIA annealing is a complex interplay of the molecular weight of the BCP system, block composition, annealing temperature, film thickness, substrate energy and the choice of the BCP system. The detailed nature of these system parameters in response to DIA is undoubtedly an interesting subject for future studies and beyond the scope of the present paper.

Based on the swelling ratio data presented in Figure 3, we find a linear relationship between SR and acetone mole fraction (x_{ace}) $SR = (h/h_0) = 2.01\ x_{ace} \pm 1.13$, valid for $x_{ace} > 0$. In a swollen homopolymer-acetone/heptane solvent mixture system, SR and x_{ace} are related as

$$\ln(\gamma_{ace}x_{ace}) = \ln\left(1 - \frac{1}{SR}\right) + \frac{1}{SR} + \frac{\chi_{polymer-acetone}}{SR^2}$$

where γ_{ace} is the activity coefficient of acetone in *n*-heptane and $\chi_{polymer-acetone}$ is the polymer-acetone interaction parameter.[33] Theoretical swelling ratio (SR) calculated from the above equation (based on mean χ parameter for the BCP) exhibits a significant nonlinear deviation from experimental data (Figure S4). However, our experimental swelling ratio is different as it is not only linear over the full range of swelling where the polymer film is intact, but also higher than the theoretical prediction, even in the low-concentration limit of x_{ace} < 0.13 where the theoretical homopolymer SR is also linear. Park et al.[33] also observed a higher swelling ratio in the solubility parameter window of their experiments. The reason for these significant deviations in a block copolymer may be due to the fact that acetone is a highly selective solvent for PMMA that leads to preferential swelling of the block and causes a high deviation in the dependence of χ parameter on solvent quality. Further, the roles of heptane−substrate and acetone−substrate interactions are not included in the calculations for the system, so we are unable describe the film dissolution regime as those interactions become important. Future simulations studies are required to address these issues.

As the solubility and stability of PS−PMMA is determined by the interplay of both PS and PMMA blocks and the substrate, control DIA studies on constituent homopolymer PMMA (14 kg/mol) and PS (35 kg/mol) films were carried out. The PMMA film dissolved in the SM at an upper bound of x_{ace} ≈ 0.4, that corresponds to the BCP film dissolution limit. Thus,

DOI: 10.1021/acsami.5b06259
ACS Appl. Mater. Interfaces 2015, 7, 21639−21645

we conclude that the BCP upper bound film stability is governed by the PMMA block, which is the strongly adsorbed block on the silicon substrate. On the other hand, the control PS homopolymer films partially dewet at and above $x_{ace} \approx 0.18$ (Figures S2 and S3), yet the BCP film remained stable apparently induced by the substrate wetting behavior of the PMMA block. For instance, no dissolution of PMMA homopolymer or PS−PMMA BCP films in the SM at $x_{ace} \approx 0.33$ is observed, confirmed by thickness measurement before and after annealing. Good substrate wetting properties of minimally one BCP block is then essential to an expanded SM processing composition spectra.

We now illustrate applicability of DIA to other block copolymer systems and PS−PMMA with different molecular parameters. Figure 4(i) shows randomly oriented, but ordered

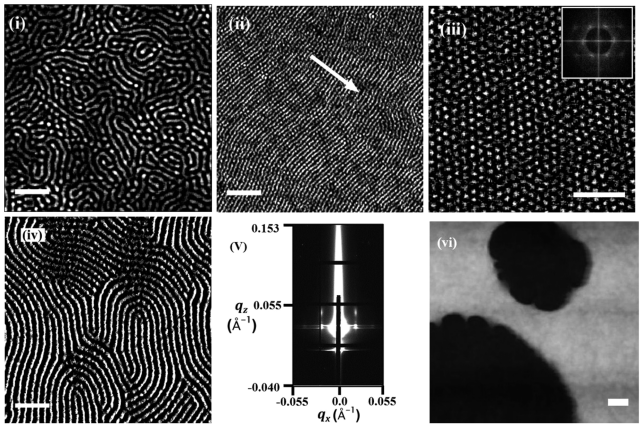

Figure 4. AFM image of films subjected to DIA: (i) *Cyl58* (dissolution was not observed because of adsorption of P2VP on native SiO_2). (ii) *Cyl47* under prepatterned PDMS. (iii) *Sph81* BCP film (inset: FFT image). (iv) *Cyl82* BCP film annealed in mixture composed of x_{ace} = 0.57. Only a residual layer is present.(v) GISAXS scattering pattern of *Cyl47* BCP film annealed in mixture composed of x_{ace} = 0.21, x_{MEK} = 0.17 (and heptane) for 1 min. (vi) *Lam66* BCP film showing island formation (scale bar: 250 nm). (Some of the images have been enhanced with image processing software for better contrast without affecting morphology.)

PS-P2VP, (40−18 kg/mol, *Cyl58*) annealed for 1 h in a solvent mixture of acetone and heptane composed of x_{ace} = 0.40. AFM peak force error image of as-cast *Cyl58* is shown in Figure S8. The P2VP block is known to adsorb on the silicon oxide substrate surface that enhances film stability for DIA processing.

To generate long-range aligned cylindrical BCP patterns, we soft mold imprinted physical patterns on the top surface of *Cyl47* (PS−PMMA) cast melt film by placing a prepatterned 5% cross-linked elastomeric PDMS stamp of period dimension, λ = 750 nm and amplitude, A = 120 nm, and thermally curing the bilayer at 180 °C in a vacuum oven for 30 min. No appreciable grain size or order was observed on film surface after pattern transfer (Figure S9). Subsequently, the patterned film (after peeling-off PDMS layer) was immersed in a SM with x_{ace} = 0.33 for 15 min. AFM shows in-plane long-range ordered cylinders (Figure 4ii) that on average are aligned orthogonal to the PDMS channel pattern shown by the arrow in a direction parallel to the pattern ridges. We conjecture that relaxation of residual stresses, developed, and trapped in film during soft pattern transfer, drives the alignment of blocks in a direction orthogonal to channel ridges upon DIA-induced molecular relaxation and ordering. Such orthogonal to pattern channel cylinder orientation has been observed in cold zone annealing (CZA) of a BCP film on a patterned substrate,[42] but in that case, it reflects an orientation based on entropic packing arrangement of the undulating cylinders.

Figure 4iii shows AFM height image of a spherical PS−PMMA (60−15 kg/mol, *Sph75*) film immersed in a ternary solvent mixture composed x_{ace} = 0.57, $x_{heptane}$ = 0.38 and $x_{toluene}$ = 0.05 for 1 h and dried on hot-plate at 60 °C. The inset 2D-FFT of the AFM image is indicative of a highly ordered hexagonal packing structure. Figure 4iv shows AFM height image of a cylindrical PS−PMMA (57−25 kg/mol, *Cyl82*) film immersed in a solvent mixture composed of x_{ace} = 0.57 for 1 h and dried on a hot-plate at 60 °C. We observe that only a residual layer (≈ 20 nm) remains in this case due to the SM quality exceeding the optimal range of "good SM" quality. Such monolayer-like patterned cylinders may however be a useful method to produce etchable BCP templates into silicon. Figure 4v shows sharp GISAXS scattering spot pattern in q_x and q_z indicative of high degree of in-plane and out-of-plane cylinder-cylinder correlation for a *Cyl47* BCP film annealed in SM of x_{ace} = 0.21, $x_{methyl\ ethyl\ ketone}$ = 0.17 for 1 min. High degree of in-plane (q_x) ordering is further corroborated by line-cut in the q_x direction, which shows diffraction up to second-order peaks compared to the as-cast film (Figure S6). Figure 4vi shows AFM height images of lamellar PS−PMMA (33−33 kg/mol, *Lam66*) film annealed in a mixture composed of x_{ace} = 0.57 and $x_{toluene}$ = 0.05 for 45 min. The distinct surface "hole topography" is clearly indicative of a well-ordered parallel lamellae film of the BCP, arising from incommensurability of total number of lamellae with film thickness, illustrating the general applicability of DIA to other morphologies in the BCP phase space.

In conclusion, we have demonstrated that DIA is a robust, convenient, and simple technique for enhancing the quality and rate of ordering in BCP thin films, potentially overcoming a number of drawbacks in thermal oven and solvent vapor annealing (SVA) processing. By comparison, DIA eliminates need for confined vapor chamber and also reduces the time required for equilibration and final quenching of swollen films in addition to reducing process control parameter usually involved with SVA. Our controlled temperature SM studies allow us to quantify changes of the energetic barrier (E_a) for long-range ordering of a cylinder forming block copolymers via DIA. As determined, DIA leads to a significantly lower E_a than the value observed in traditional oven annealing of cast BCP films and more akin to very high temperature BCP annealing. We find that the DIA method is quite versatile and illustrates the application of this method to other BCP systems and type, exhibiting different types of ordering and for different solvent mixture combinations and compositions to gain insight into the underlying principles governing this process.

■ ASSOCIATED CONTENT

Supporting Information

The Supporting Information is available free of charge on the ACS Publications website at DOI: 10.1021/acsami.5b06259.

Figures S1−S9 (PDF)

DOI: 10.1021/acsami.5b06259
ACS Appl. Mater. Interfaces 2015, 7, 21639−21645

AUTHOR INFORMATION

Corresponding Author

*E-mail: alamgir@uakron.edu.

Notes

The authors declare no competing financial interest.

ACKNOWLEDGMENTS

We acknowledge the Department of Energy, Basic Energy Sciences via Grant DE-SC0005364 for support of the phase separation morphology aspect of work. The directed-assembly component of the work was supported by the National Science Foundation via Grant NSF DMR-1411046. A.M. would like to thank Dr. Kevin Yager, Prof. Brian Berry, Dr. Mesfin Tsige, Saumil Samant, and Dr. Ankur Verma for fruitful discussions. A.M. also acknowledges Namrata Salunke for proof reading the manuscript. Use of the National Synchrotron Light Source, Brookhaven National Laboratory, was supported by the U.S. Department of Energy, Office of Science, Office of Basic Energy Sciences, under Contract DE-AC02-98CH10886. Certain equipment, instruments, or materials are identified in this paper in order to adequately specify the experimental details. Such identification does not imply recommendation by the NIST nor does it imply the materials are necessarily the best available for the purpose.

ABBREVIATIONS

BCP, block copolymer

AFM, atomic force microscopy

REFERENCES

(1) Sanders, D. P. Advances in Patterning Materials for 193 nm Immersion Lithography. *Chem. Rev.* **2010**, *110*, 321−360.

(2) Chai, J.; Wang, D.; Fan, X.; Buriak, J. M. Assembly of Aligned Linear Metallic Patterns on Silicon. *Nat. Nanotechnol.* **2007**, *2*, 500−506.

(3) Varghese, J.; Ghoshal, T.; Deepak, N.; O'Regan, C.; Whatmore, R. W.; Morris, M. A.; Holmes, J. D. Fabrication of Arrays of Lead Zirconate Titanate (PZT) Nanodots via Block Copolymer Self-Assembly. *Chem. Mater.* **2013**, *25*, 1458−1463.

(4) Xiao, S.; Yang, X.; Lee, K. Y.; ver der Veerdonk, R. J. M.; Kuo, D.; Russell, T. P. Aligned Nanowires and Nanodots by Directed Block Copolymer Assembly. *Nanotechnology* **2011**, *22*, 305302.

(5) Park, S.; Wang, J.-Y.; Kim, B.; Russell, T. P. From Nanorings to Nanodots by Patterning with Block Copolymers. *Nano Lett.* **2008**, *8*, 1667−1672.

(6) Xu, J.; Hong, S. W.; Gu, W.; Lee, K. Y.; Kuo, D. S.; Xiao, S.; Russell, T. P. Fabrication of Silicon Oxide Nanodots with an Areal Density beyond 1 Teradots $Inch^{-2}$. *Adv. Mater.* **2011**, *23*, 5755−5761.

(7) Liu, Z.; Huang, H.; He, T. Large-Area 2D Gold Nanorod Arrays Assembled on Block Copolymer Templates. *Small* **2013**, *9*, 505−510.

(8) Thurn-Albrecht, T.; Schotter, J.; Kästle, G. A.; Emley, N.; Shibauchi, T.; Krusin-Elbaum, L.; Guarini, K.; Black, C. T.; Tuominen, M. T.; Russell, T. P. Ultrahigh-Density Nanowire Arrays Grown in Self-Assembled Diblock Copolymer Templates. *Science* **2000**, *290*, 2126−2129.

(9) Lei, L.; Xia, Y.; Chen, X.; Shi, S. Long-Range-Ordered, Hexagonally Packed Nanoporous Membranes from Degradable-Block-Containing Diblock Copolymer Film Templates. *J. Appl. Polym. Sci.* **2014**, *131*, 39638.

(10) Hahn, J.; Filiz, V.; Rangou, S.; Clodt, J.; Jung, A.; Buhr, K.; Abetz, C.; Abetz, V. Structure Formation of Integral-Asymmetric Membranes of Polystyrene-*block*-Poly(ethylene oxide). *J. Polym. Sci., Part B: Polym. Phys.* **2013**, *51*, 281−290.

(11) Fang, Z.; Zhu, X. Plasmonics in Nanostructures. *Adv. Mater.* **2013**, *25*, 3840−3856.

(12) Lee, J. Y.; Lee, J.; Jang, Y. J.; Lee, J.; Jang, Y. H.; Kochuveedu, S. T.; Lee, S. S.; Kim, D. H. Plasmonic Nano-Necklace Arrays via Reconstruction of Diblock Copolymer Inverse Micelle Nanotemplates. *Soft Matter* **2011**, *7*, 57−60.

(13) Hassan, N.; Cabuil, V.; Abou-Hassan, A. Assembling Magneto-Plasmonic Microcapsules Using a Microfluidic Device. *Chem. Commun.* **2013**, *49*, 412−414.

(14) Naik, G. V.; Shalaev, V. M.; Boltasseva, A. Alternative Plasmonic Materials: Beyond Gold and Silver. *Adv. Mater.* **2013**, *25*, 3264−3294.

(15) Marencic, A. P.; Adamson, D. H.; Chaikin, P. M.; Register, R. A. Shear Alignment and Realignment of Sphere-Forming and Cylinder-Forming Block-Copolymer Thin Films. *Phys. Rev. E* **2010**, *81*, 011503.

(16) Zhang, R.; Singh, G.; Dang, A.; Dai, L.; Bockstaller, M. R.; Akgun, B.; Satija, S.; Karim, A. Nanoparticle-Driven Orientation Transition and Soft-Shear Alignment in Diblock Copolymer Films via Dynamic Thermal Gradient Field. *Macromol. Rapid Commun.* **2013**, *34*, 1642−1647.

(17) Kim, S. Y.; Gwyther, J.; Manners, I.; Chaikin, P. M.; Register, R. A. Metal-Containing Block Copolymer Thin Films Yield Wire Grid Polarizers with High Aspect Ratio. *Adv. Mater.* **2014**, *26*, 791−795.

(18) Wu, M.; Register, R.; Chaikin, P. Shear Alignment of Sphere-Morphology Block Copolymer Thin Films with Viscous Fluid Flow. *Phys. Rev. E* **2006**, *74*, 040801.

(19) Bita, I.; Yang, J. K. W.; Jung, Y. S.; Ross, C. A.; Thomas, E. L.; Berggren, K. K. Graphoepitaxy of Self-Assembled Block Copolymers on Two-Dimensional Periodic Patterned Templates. *Science* **2008**, *321*, 939−943.

(20) Tavakkoli K G, A.; Gotrik, K. W.; Hannon, A. F.; Alexander-Katz, A.; Ross, C. A.; Berggren, K. K. Templating Three-Dimensional Self-Assembled Structures in Bilayer Block Copolymer Films. *Science* **2012**, *336*, 1294−1298.

(21) Choi, H. K.; Gwyther, J.; Manners, I.; Ross, C. A. Square Arrays of Holes and Dots Patterned from a Linear ABC Triblock Terpolymer. *ACS Nano* **2012**, *6*, 8342−8348.

(22) Kulkarni, M.; Yager, K.; Sharma, A.; Karim, A. Combinatorial Block Copolymer Ordering on Tunable Rough Substrates. *Macromolecules* **2012**, *45*, 4303−4314.

(23) Sinturel, C.; Vayer, M.; Morris, M.; Hillmyer, M. A. Solvent Vapor Annealing of Block Polymer Thin Films. *Macromolecules* **2013**, *46*, 5399−5415.

(24) Albert, J. N. L.; Epps, T. H., III Self-Assembly of Block Copolymer Thin Films. *Mater. Today* **2010**, *13*, 24−33.

(25) Ruiz, R.; Bosworth, J.; Black, C. Effect of Structural Anisotropy on the Coarsening Kinetics of Diblock Copolymer Striped Patterns. *Phys. Rev. B: Condens. Matter Mater. Phys.* **2008**, *77*, 054204.

(26) Kim, E.; Ahn, H.; Park, S.; Lee, H.; Lee, M.; Lee, S.; Kim, T.; Kwak, E.-A.; Lee, J. H.; Lei, X.; Huh, J.; Bang, J.; Lee, B.; Ryu du, Y. Directed Assembly of High Molecular Weight Block Copolymers: Highly Ordered Line Patterns of Perpendicularly Oriented Lamellae with Large Periods. *ACS Nano* **2013**, *7*, 1952−1960.

(27) Gotrik, K. W.; Ross, C. A. Solvothermal Annealing of Block Copolymer Thin Films. *Nano Lett.* **2013**, *13*, 5117−5122.

(28) Verma, A.; Sharma, A. Organization in Highly Confined Soft Matter to Sub-100 nm Scales: Nanolens-Arrays by Spinodal Instability of Thin Polymer Films for High-Resolution Optical Imaging. *Curr. Sci.* **2013**, *104*, 1037−1045.

(29) Xu, L.; Sharma, A.; Joo, S. W. Dewetting of Stable Thin Polymer Films Induced by a Poor Solvent: Role of Polar Interactions. *Macromolecules* **2012**, *45*, 6628−6633.

(30) Verma, A.; Sharma, A. Submicrometer Pattern Fabrication by Intensification of Instability in Ultrathin Polymer Films Under a Water−Solvent Mix. *Macromolecules* **2011**, *44*, 4928−4935.

(31) Verma, A.; Sharma, A. Enhanced Self-Organized Dewetting of Ultrathin Polymer Films under Water-Organic Solutions: Fabrication of Sub-Micrometer Spherical Lens Arrays. *Adv. Mater.* **2010**, *22*, 5306−5309.

(32) Verma, A.; Sharma, A. Self-Organized Nano-Lens Arrays by Intensified Dewetting of Electron Beam Modified Polymer Thin-Films. *Soft Matter* **2011**, *7*, 11119−11124.

DOI: 10.1021/acsami.5b06259
ACS Appl. Mater. Interfaces 2015, 7, 21639−21645

(33) Park, W. I.; Kim, J. M.; Jeong, J. W.; Jung, Y. S. Deep-Nanoscale Pattern Engineering by Immersion-Induced Self-Assembly. *ACS Nano* **2014**, *8*, 10009−10018.
(34) Hansen, C. M.; Smith, A. L. Using Hansen Solubility Parameters to Correlate Solubility of C_{60} Fullerene in Organic Solvents and in Polymers. *Carbon* **2004**, *42*, 1591−1597.
(35) Li, W.; Nealey, P. F.; de Pablo, J. J.; Müller, M. Defect Removal in the Course of Directed Self-Assembly Is Facilitated in the Vicinity of the Order-Disorder Transition. *Phys. Rev. Lett.* **2014**, *113*, 168301.
(36) Koenig, J. L. Dissolution of Symmetric Diblock Copolymers with Neutral Solvents, a Selective Solvent, a Nonsolvent, and Mixtures of a Solvent and Nonsolvent Monitored by FT-IR Imaging. *Macromolecules* **2003**, *36*, 4851−4861.
(37) Berry, B. C.; Bosse, A. W.; Douglas, J. F.; Jones, R. L.; Karim, A. Orientational Order in Block Copolymer Films Zone Annealed below the Order-Disorder Transition Temperature. *Nano Lett.* **2007**, *7*, 2789−2794.
(38) Majewski, P. W.; Yager, K. G. Millisecond Ordering of Block Copolymer Films via Photothermal Gradients. *ACS Nano* **2015**, *9*, 3896−3906.
(39) Hahm, J.; Sibener, S. J. Time-Resolved Atomic Force Microscopy Imaging Studies of Asymmetric PS-b-PMMA Ultrathin Films: Dislocation and Disclination Transformations, Defect Mobility, and Evolution of Nanoscale Morphology. *J. Chem. Phys.* **2001**, *114*, 4730.
(40) Horinouchi, A.; Yamada, N. L.; Tanaka, K. Aggregation States of Polystyrene at Nonsolvent Interfaces. *Langmuir* **2014**, *30*, 6565−6570.
(41) Atarashi, H.; Morita, H.; Yamazaki, D.; Hino, M.; Nagamura, T.; Tanaka, K. Swelling Structure of Thin Poly(methyl methacrylate) Films in Various Alkyl Length Alcohols. *J. Phys. Chem. Lett.* **2010**, *1*, 881−885.
(42) Berry, B. C.; Singh, G.; Kim, H.-C.; Karim, A. Highly Aligned Block Copolymer Thin Films by Synergistic Coupling of Static Graphoepitaxy and Dynamic Thermal Annealing Fields. *ACS Macro Lett.* **2013**, *2*, 346−350.

DOI: 10.1021/acsami.5b06259
ACS Appl. Mater. Interfaces 2015, 7, 21639−21645